Reactions and energy absorption of trees subject to rockfall: a detailed assessment using a new experimental method

TOR LUNDSTRÖM,[1,2,3] MARTIN J. JONSSON,[1] AXEL VOLKWEIN[1] and MARKUS STOFFEL[3]

[1] *WSL, Swiss Federal Institute for Snow and Avalanche Research SLF, CH-7260 Davos, Switzerland*

[2] *Corresponding author (t.lundstroem@slf.ch)*

[3] *Laboratory of Dendrogeomorphology, University of Fribourg, 1700 Fribourg, Switzerland*

Summary A new method for investigating the detailed reaction and the energy absorption of trees during a rock impact was developed and applied to 15 subalpine Norway spruce (*Picea abies* L. Karst) trees. A wedge-shaped trolley, guided by prestressed steel wires, was mounted on a forested slope to simulate a falling rock. The trolley accelerates down the wires and hits a tree at a preselected stem height with variable energies. The tree displacements and accelerations during the impact were recorded to determine reactions and energy absorption for the stem, root–soil system, crown and the entire tree. Trees absorbed the kinetic energy of the trolley rapidly by mobilizing strain and inertia forces close to the impact location in the stem and the root–soil system. This energy was then gradually dissipated all over the tree through permanent deformations and damping. The stem assimilated more energy than the root–soil system. The tree's energy absorption capacity was limited by stem-bending stresses at impact height, by shear stresses at the stem base and by lack of resistance of the root–soil anchorage. It was positively and exponentially related to stem diameter at breast height and negatively related to impact height. The field experiment enabled a physical description of how a tree reacts to a rock impact and highlighted the most important and critical components of the tree for its energy absorption. Such descriptions should help make computer simulations of rock–forest interrelations more precise and thus improve management strategies to ensure that forests can provide protection against rockfall.

Keywords: biomechanics, dynamics, energy balance, finite-element tree model, spatiotemporal analysis, stem deflection.

Introduction

Mountain forests provide a form of natural protection against falling rocks. Although rockfall models are commonly used to predict the trajectory, kinetic energy and run-out distance of the rocks (Zinggeler et al. 1991, Dorren and Seijmonsbergen 2003), less empirical information about the phenomenon of rock impact on trees is available (Mizuyama and Narita 1988, Dorren and Berger 2006). To determine the protective capacity of forests and to develop effective forest management strategies, it is essential to understand the mechanical processes of the tree–rock interaction. This understanding provides a basis for defining the forest parameters affecting the energy absorption of trees and the extent to which such parameters can be modified by human intervention.

A kinematical description of a falling rock moving through a mountain forest is complex. Rocks have a wide variety of shapes and forms, making it difficult to predict the center of mass and moments of inertia accurately. Falling rocks tend to rotate around the smaller inertia axis, contacting the ground in a jumping and sliding motion (Azzoni and Defreitas 1995). These factors reduce the rotational energy of the rock. In the field, this energy is negligible (Dorren and Berger 2006), unlike observations in the laboratory (Chau et al. 2002, Heidenreich and Labiouse 2004). Typical translational velocities are in the order of 10–30 m s^{-1} (Krummenacher and Keusen 1997). Recent investigations of rockfall scars on tree stems (Perret et al. 2004, Stoffel et al. 2006) indicate that impact heights of 1.2 ± 0.5 m are common. Experiments with rocks thrown down a forested slope (Dorren and Berger 2006) indicate that the kinetic rock energy is absorbed by the entire tree (root–soil anchorage, stem and crown). This energy absorption is, as for any structure subject to heavy dynamic loading, related to inertia, reversible and permanent deformation, friction and damping. The latter three terms describe dissipation of energy, i.e., how the energy changes form (e.g., into heat). Energy absorption, a generic name for energy uptake, is a sine qua non for energy dissipation. The focus of this paper is therefore on energy absorption.

From a mechanical point of view, trees are highly complex. Their anisotropically organized structure depends on

growth conditions (Brüchert et al. 2000, Polomski and Kuhn 2001). Because of these natural variations, it is difficult to predict the reaction of a tree to a rock impact, and trees can be expected to absorb energy in different ways and in varying amounts. Energy absorption due to deformation depends on mechanical properties, e.g., how stress develops with strain. For coniferous wood, the stress–strain time course is strain-rate dependent (Bragov and Lomunov 1997). Strain rates above 5 and $100 \ s^{-1}$ yield relatively higher stress perpendicular and parallel to the wood fiber, respectively (Murray 2003). Some of the mechanical properties of tree components likely to play important roles in the rock–tree interaction have been described, e.g., the bending of the stem (Lundström et al. 2008b) and of the root–soil system (Lundström et al. 2007b). However, how these components behave and how they interact during a rock impact on the tree have been largely unexplored.

To better understand the interaction between an impacting rock and a tree, a new experimental method was developed to explore: (1) How a tree reacts to a rock impact? (2) How the kinetic energy of the rock is absorbed in the tree? (3) How much energy a tree can assimilate without falling over? The method included investigating living trees in the forest, carrying out full-scale rock–tree impact tests and analyzing the field records with a simplified finite-element tree model. In this study, the method was applied to 15 subalpine Norway spruce trees.

Materials and methods

Test trees

Fifteen Norway spruce (*Picea abies* L. Karst) trees were selected as being representative of protective forests in the Alps, in terms of tree size and growth conditions (Table 1). All trees appeared healthy, except Tree A7 that had some rot in the center of the stem along its base. All the 15 trees grew in two closely situated subalpine forests near Davos, Switzerland, with Site A at 46°47′N, 9°48′W and 1770 m a.s.l. and Site B at 46°47′N, 9°50′W and 1680 m a.s.l. The ground of Site A faces ESE with a slope of 30°. It has a shallow B-horizon (5–35 cm) of dystric Cambisol (taxonomy according to FAO 1998) with frequent stones. The ground of Site B faces NNW with a slope of 35°. Its B-horizon is also a dystric Cambisol, but it is less shallow (10–40 cm) and has less frequent stones. Mean stocking density was 500 trees ha⁻¹ in both stands. Rocks falling through the forests of the study area generally have low kinetic energy (< 100 kJ) and mass (< 1000 kg). The periods before and during the tests in summer 2003 and 2004 were slightly warmer and drier than normal (+ 12 versus + 10 °C and 110 versus 120 mm month⁻¹). Further relevant site climate data are presented in Lundström et al. (2008a). Symbols used in this paper are summarized in the Appendix (Table A1).

Table 1. Tree characteristics relevant to this study: DBH = diameter at breast height, i.e., at stem height $z = 1.3$ m; H = tree height; L_c = crown length; m_{tree} = total aboveground tree mass; Age = cambial age; RW = annual ring width, where $_i$ refers to the mean of the inner 75% radial part of the stem cross section and $_o$ to the mean of the remaining outer radial part; ρ_w = stem bulk density; σ_{max} = bending strength (also called modulus of rupture); MOE = bending elasticity (or modulus of elasticity); τ_{max} = shearing strength and G = shearing elasticity.

Site and tree no.	DBH (m)	H (m)	L_c/H (–)	m_{tree} (kg)	Age[1] (years)	RW_i[1] (mm)	RW_o[1] (mm)	ρ_w[1] (kg m⁻³)	σ_{max}[1] (MPa)	MOE[1] (GPa)	τ_{max}[1] (MPa)	G[1] (MPa)
A1	0.35	26	0.53	950	125	2.1	1.4	830	57.8	11.8	2.6	530
A2	0.48	33	0.88	2430	218	1.9	1.2	850	49.0	12.8	2.7	540
A3	0.44	30	0.92	1970	193	1.5	0.9	880	44.4	14.5	3.0	580
A4	0.58	35	0.83	2820	272	0.9	0.6	930	57.1	17.0	3.7	670
A5	0.43	28	0.78	1480	184	1.1	0.9	870	54.6	14.5	3.5	630
A6	0.22	21	0.76	360	110	1.5	0.7	880	59.7	16.5	3.1	590
A7	0.38	23	0.66	1180	132	1.8	1.3	840	54.2	12.3	2.8	550
A8	0.35	26	0.80	910	116	1.6	1.2	830	53.3	12.8	3.0	580
A9	0.50	35	0.80	2770	273	1.3	1.3	880	49.0	12.3	3.2	600
A10	0.51	32	0.88	2720	271	0.9	1.2	900	46.5	12.8	3.8	670
B1	0.40	31	0.78	1640	170	1.5	1.2	850	51.2	12.8	3.0	580
B2	0.39	34	0.56	1600	175	1.7	0.8	860	61.6	15.3	2.9	570
B3	0.49	33	0.49	2030	221	1.7	0.8	870	63.1	15.3	2.9	570
B4	0.43	32	0.47	1620	179	1.3	1.0	860	60.5	13.9	3.3	610
B5	0.43	32	0.78	1820	174	1.4	1.1	860	50.0	13.3	3.1	590

[1] Value of the fresh stem section at $z = 2$ m.

Test procedure

Each test tree was investigated before and after the destructive impact experiment (Table 2). In the impact experiment (Step 4, Table 2), the rock was simulated with a wedge-front-shaped trolley (Figure 1A), guided by two steel wires on each side of the test tree (Figure 1B), prestressed with about 50 kN between two groups of trees. The trolley front is made of solid steel with a rough surface, representing a coefficient of kinetic friction of 0.3 against green wood (determined experimentally in the laboratory). Deposits of rocks originating from rockfall in the region of Davos were investigated to determine a typical rock edge. This was found to be right-angled, but slightly rounded, so the trolley front edge was designed with an angle of 90°, and rounded-off at a 20 mm radius. The trolley mass is adjustable from 292 to 892 kg with 50 and 100 kg concrete blocks positioned behind the front. The wire positions can be adjusted in height and sideways with steel supports on the lower and the upper wire ends. A third wire is attached to the back of the trolley to winch it up the wires to the starting position with a jeep driven on a forest road. There, it is released and accelerated down the wires to impact the test tree. The vertical drop that determines the impact speed and the mass of the trolley was adjusted to the energy required to make the tree just fall over. This energy was estimated on the basis of previous tests, data from the investigation Steps 1–3 (Table 2) and displacement-based simulations with the tree model used for the impact analysis (cf. section entitled *Tree model and its mechanical properties*). The highest achievable kinetic energy depends on the wire length and slope angle. With a maximum effective wire length of 55 m (for practical reasons) and a mean slope of 30°, this energy is about 250 kJ. A steel wire protection net was mounted on the lower side of the tree in case the trolley was not stopped by the tree.

Data acquisition of the impact test

Ten accelerometers (ABM-25-4-20, AMOS Sensoren & Meßtechnik, Mannheim, Germany) and four digital video
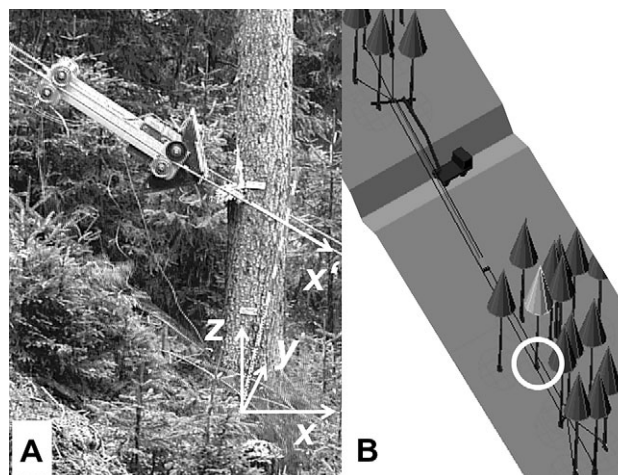

Figure 1. (A) The trolley, pictured shortly after impact with the test tree, is guided by four wheels on each side that grip the prestressed steel wires. (B) The trolley runs down the steel wires, which are mounted between two groups of trees, to impact the tree (circled).

cameras (two Sony DCR-TRV900E, Sony Corp., Tokyo, Japan, and two Redlake MotionScope-PCI, Roper Industries Inc., Duluth, GA) were connected to a data logger (DAQPad-6052E, NI Corp., Austin, TX). To minimize the influence of magnetic fields and temperature changes, all 14 devices were supplied with current. The data logger was connected by a firewire (IEE394) to a laptop computer that controlled and synchronized the measuring devices using a LabView-program (NI Corp.). On the trolley, two accelerometers measured in the vertical plane ($y = 0$) (Figure 1A): one in the direction of the wire (x') and one perpendicular to it (z'), both with a range of ± 500 m s^{-2}. Eight accelerometers were positioned on the downhill side of the stem at relative tree heights of 2% (x/y; $\pm 500/200$ m s^{-2}), 7% (x; ± 500 m s^{-2}), 20% (x; ± 200 m s^{-2}), 35% (x; ± 200 m s^{-2}), 53% (x; ± 100 m s^{-2}) and 75% (x/y; $\pm 100/50$ m s^{-2}), where x and y

Table 2. Successive steps for investigating trees subject to rock impact. The methods or data sources used are given in parentheses.

Step	Description
1	Characterization of the tree: species, DBH, estimated H (with clipper, measuring tape and hypsometer), vitality (optically), soil type (data bank or in situ sample)
2	Swaying test: determination of natural swaying frequencies and damping (Jonsson et al. 2007)
3	Winching test: determination of the initial rotational stiffness of the root–soil system (Jonsson et al. 2006)
4	Destructive impact test. If this test does not make the tree fall, the entire tree is winched down
5	Measurements of the lying tree: the geometry and mass of the stem and the crown (Lundström et al. 2008a) and the dimensions and shape of the root–soil plate (Lundström et al. 2007a)
6	Laboratory investigations of stem and soil samples: determination of the annual ring width RW, knottiness and stem bulk density ρ_w in stem disks from close below and above the impact height, and at least four additional stem heights above it (Lundström et al. 2008b); determination of the bulk density, moisture content and granulometry of the soil in the root–soil plate (according to standard procedures)
7	Laboratory tests of the local penetration of a rock front into the fully supported stem, thus with no stem-bending. The test setup, which uses the same impact trolley as in Step 4, is described in: http://www.wsl.ch/forschung/forschungsprojekte/Treestability/local-impact_EN [accessed July 9, 2008]

indicate their measurement directions. All accelerometers sampled at a rate of 10 kHz. Records in the y-direction were made to verify that the energy analysis was restricted to the x–z-plane. Two cameras filmed the lower part of the tree with a frequency of 25 (Sony) and 250 Hz (Redlake), respectively. The latter also detected the impact velocity of the trolley. The two remaining cameras film the upper part of the tree with the same frequencies. The data logger was triggered to start sampling accelerations and images as the trolley passed a photocell (Polifemo, Microgate, Italy) positioned some meters above the test tree.

Displacement analysis of the impact test

The displacements in time of the tree and the trolley, in the x- and y-directions, were detected from the 250 Hz video image series (480 × 420 pixels). For this detection, two software programs were used: (1) WinAnalyse (DEL Imaging Systems, LLC, Cheshire, CT), which allows point-tracking, with automatic descriptions of displacements, velocities and accelerations, but which does not account for the geometrical and the optical image distortion and (2) Stemtrack, especially developed for detecting tree deflections with high precision. It describes stem deflection with polynomials of stem height and time $x(z, t)$ and takes the image distortion fully into account. If a 30-m high tree is captured entirely in two 250 Hz-images merged vertically, the precision in stem deflection is about 5 cm (cf. Lundström et al. 2007a). For technical information, see http://www.wsl.ch/forschung/forschungsunits/lawinen/downloads/Stemtrack.pdf [accessed July 9, 2008]. WinAnalyse analyzed the local penetration of the trolley front into the stem and Stemtrack analyzed the deflections of the entire tree stem. Here, the deflections detected from the picture series filmed with the lower and the upper cameras were merged. To increase the number of deflection estimates in time, i.e., to obtain stem deflections between those detected with Stemtrack, the recorded accelerations were integrated twice according to Newmark's linear acceleration method (Chopra 1995). The latter high-frequency deflections (10 kHz) were forced to coincide with the deflections of Stemtrack (250 Hz) at the same time step. Deflections obtained on the basis of acceleration records only would be erroneous because of the accumulated errors resulting from the dynamical drift and offset of the sensors. The 25 Hz series (768 × 576 pixels) were analyzed in the same way as the 250 Hz series and provided a control function of every 10th image from the 250 Hz series.

A precise description of the stem deflections and deformations of the root–soil system during the impact is essential to accurately determine the tree's reaction and energy absorption. The following description has proved to be precise and practical:

$$x(z,t) = a_n(t) \cdot z^n + a_{n-1}(t) \cdot z^{n-1} \cdot \ldots \cdot a_1(t) \cdot z^1 + a_0(t),$$
$$(1)$$

where $x(z, t)$ is the cylindrical center of the stem, describing a line from the stem base to the tree top (Figure 3A); $a(t)$ is a polynomial coefficient at time t and superscript n is a
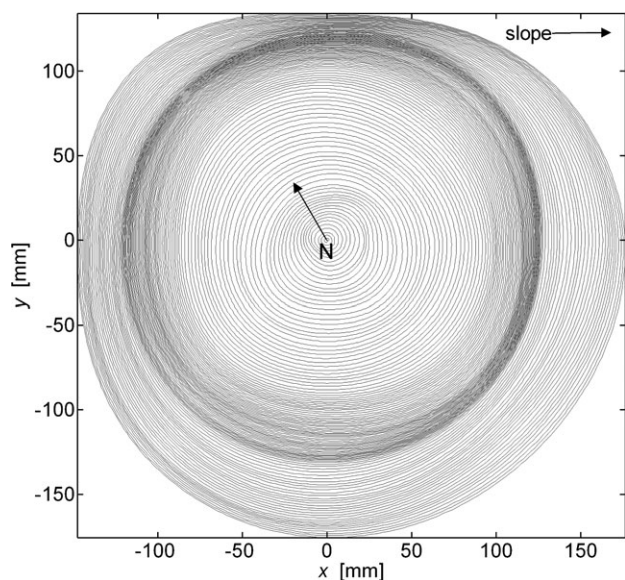

Figure 2. Digitized stem disk with annual rings sampled at a stem height of 2.0 m from Tree A8. The x-axis (to the right in the figure) corresponds to the slope and impact direction and faces ESE. The preferential azimuthal stem growth is found in the orientations facing the slope and the south. N (in the pith) indicates the north.
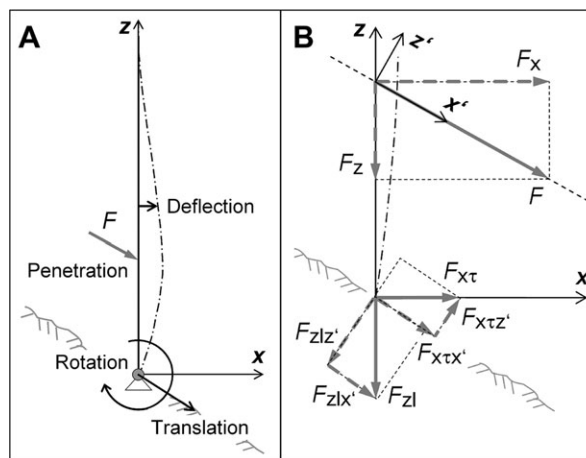

Figure 3. (A) Simplified model of the tree used to analyze the tree reaction and the energy absorption caused by stem deflection, local penetration of the trolley front into the stem, and rotation and translation of the root–soil system. (B) Decomposition of the force F applied by the trolley to the stem into vector components. Abbreviations: τ denotes the transverse (shear) forces; l denotes the longitudinal (compressive or tension) forces effectively transmitted by the stem to the ground; $F_{x\tau x'}$ and $F_{x\tau z'}$ are components of $F_{x\tau}$; and $F_{zlx'}$ and $F_{zlz'}$ are components of F_{zl}. The magnitudes of $F_{x\tau}$ and F_{zl} depend on how intensively the energy is absorbed by the stem.

polynomial degree, so that the stem deflection, and thus the tree reaction, is reproduced accurately. During the short time interval of energy absorption analyzed, the vertical stem deflections are small compared with the lateral stem deflections and are therefore neglected. To facilitate the analysis, the initial positions for x and y are set to 0. The stem line thus intersects the ground at $(x, y, z) = (0, 0, 0)$, from where it describes a vertical up to the top of the tree. The location of the center of rotation of the root–soil system approximates $(x, y, z) = (0, 0, 0)$ (cf. Lundström et al. 2007b). Consequently, the rotation of the root–soil system equals the rotation at the stem base ($z = 0$). The last polynomial term, $a_0(t)$, divided by the cosine of the slope angle, describes the translation of the root–soil system in the slope direction, and $a_1(t)$ describes its rotation (i.e., the stem-base inclination) as a function of time. The strain rate for the roots is estimated from the time courses of a_0 and a_1, and considering that an equivalent root length of at least 0.5 m is subjected to strain. All second derivatives of Eq. (1) with respect to t describe accelerations. The second derivative of Eq. (1) with respect to z describes the stem curvature and the third derivative describes the change in this curvature. The two derivates are related to the bending strain in the outermost wood fiber and to the mean shear strain of the cross section, ε and γ, respectively:

$$\varepsilon(z) = \frac{D(z)}{2} \cdot \frac{d^2x}{dz^2};$$

$$\gamma(z) = \frac{MOE(z) \cdot I(z)}{G(z) \cdot A_S(z)} \cdot \frac{d^3x}{dz^3}, \qquad (2)$$

where $D(z) = D_1(z) - B(z)$ is stem diameter under bark, $D_1(z)$ is stem diameter on bark, $B(z)$ is double bark thickness, $MOE(z)$ is the bending modulus of elasticity, $I(z) = \pi(D(z)^4/64)$ is the cross-sectional moment of inertia, $G(z)$ is the shear modulus of elasticity, $A_s(z) = A(z)/1.1$ is the effective shear area of the actual cross-sectional area, $A(z) = \pi(D(z)^2/4)$. The strain rates of stem-bending and shear are determined by analyzing the time course of Eq. (2).

Tree model and its mechanical properties

To analyze the reaction and the energy absorption of the tested tree on impact, a simplified finite-element model of the test tree was coded in Matlab 7.0 (MathWorks, Inc., Natick, MA). The model consists of 100 equally long beam elements (of Timoshenko type, cf. Cook et al. 2002), with the lowermost element flexibly clamped to the ground. The elements are attributed mechanical properties on the basis of Steps 1, 3 and 5–7 in Table 2 and the values in Table 1, with all geometrical properties and density as polynomials of height. The tree model is similar to that described by Lundström et al. (2008a), with three exceptions: no geometrical nonlinear effects are considered; the maximum resistive turning moment of the root–soil system

M^0_{max} is predicted (according to Lundström et al. 2007b) and the stem-bending is simplified (according to Lundström et al. 2008b). The pure bending stress σ is thus ideally elastic from the bending strain $\varepsilon = 0$ to $\varepsilon = \varepsilon_1 = 0.91$ $\sigma_{max}(z)/MOE(z)$, and then ideally plastic from ε_1 to the bending failure at $\varepsilon = 2.4\varepsilon_1$, with the actual σ_{max} occurring at $\varepsilon = 2.0\varepsilon_1$ (see Tables 1 and A1 for symbol explanations). The bending shear stress γ has its respective shear strain limits $\gamma_1 = 0.91\gamma_{max}(z)/G(z)$ and $1.4\gamma_1$ (Wessolly and Erb 1998, Dinwoodie 2000). The $\sigma_{max}(z)$ and $MOE(z)$ of the model tree is each defined by a spline (cubic spline interpolation, Matlab) covering $0 < z < H$, calculated (according to Lundström et al. 2008b) on the basis of the annual ring width (RW) and the knottiness in the stem disks sampled from the tree.

Some of the trees tested displayed fairly asymmetrically grown stems (Figure 2). Therefore a comparison was made between the bending properties calculated for symmetrical (geometric mean) and asymmetrical (actual) stem disks sampled at $z = 2.0$ m. The cross section was divided into circle segments with the thickness of one annual ring and an opening angle of 1°, and MOE and σ_{max} were calculated in all bending azimuths (0–359°) on the basis of Lundström et al. (2008b) and the parallel-axis theorem. The difference between the asymmetric and symmetric disks was at the most 3% for MOE and 2% for σ_{max}. Calculated on the same basis for the two related geometrical properties I and the section modulus $2(I/D)$, the corresponding differences were at most 13% and 8%, respectively. These four differences averaged for all trees were about a third as great. Because these discrepancies have little influence on the aims of our study, the analysis was simplified by considering all bending properties to be independent of azimuth. Finally, the properties of growth in the stem center varied little with height. Therefore, $G(z)$ and $\tau_{max}(z)$ were approximated and treated as constants (Table 1), estimating τ_{max} according to Lundström et al. (2008b) and $G = 118\tau_{max} + 400$ (MPa) (Kollmann 1968).

Energy analysis of the impact test

To determine how the energy applied by the impact trolley is absorbed by the tree over time and space, the energy balance for the trolley–tree interaction was considered, applying the equation of motion of an inelastic system (Clough and Penzien 1993). Here, all the relevant forces and stresses acting in the system (Figure 3A) were multiplied by their displacements, computed for every time step (set to 1 ms) from the first contact between the trolley and the tree stem ($t = 0$) until the intensity of the tree's energy absorption reaches a value close to zero, i.e., during the period T_{abs}. The energy intensity (J s^{-1} or W) applied by the trolley to the tree is:

$$dW_{app} = -m_{trolley} \cdot \left(\frac{d^2x'}{dt^2} \cdot dx' + \frac{d^2x'}{dt^2} \cdot dz' \right), \qquad (3)$$

Table 3. Groups of energy absorption phenomena of the tree, their descriptions and corresponding equation (Eq.).

Group	Description	Eq.
I	Deformation of stem in bending, through	4
Ia	pure bending in the elastic domain	
Ib	pure bending in the plastic domain	
Ic	longitudinal shearing in the elastic domain	
Id	longitudinal shearing in the plastic domain	
II	Inertia of stem in x-wise deflection	5
III	Deformation of stem by local penetration[1]	6
IV	Deformation of root–soil system in rotation	7
V	Inertia of root–soil system in rotation	8
VI	Deformation of root–soil system in translation	9
VII	Inertia of root–soil system in translation	10
VIII	Diverse losses	–

[1] Penetration by the trolley front (simulated rock edge) into the stem.

where $m_{trolley}$ is the total mass of the trolley and x' and z' are displacements of the trolley's center of gravity (Figure 3B). Equation (3) assumes that the energy absorbed z'-wise is used to deform the tree and not to push the wires, i.e., that the wedge front does not just slip down on the tree stem in the z'-direction.

The way the tree structure absorbs dW_{app} was categorized into eight groups of absorption phenomena (I–VIII, Table 3), which are incorporated in the code for the tree model. When provided with records of displacements and accelerations (Eq. (1)), the code calculates the energy intensity dW and the energy absorption W for each phenomenon and for the entire tree, where W is dW integrated with respect to time. The energy absorbed by the tree through damping can be ignored for the impact event, because T_{abs} is short compared with the first vibration frequencies of the tree structure (Clough and Penzien 1993). In contrast, the elastic strains and inertia forces need to be considered in the energy analysis during T_{abs}, although the related energies will, after T_{abs}, dissipate in damping or plastic strain throughout the tree. The energy intensities, dW, for each of the eight phenomena are described below.

Energy is required to deform the stem in bending (I, Table 3). In the elastic domain (Ia and Ic), this is described by Sundström (1998), and is reproduced here slightly rearranged

$$dW = W(t + dt) - W(t);$$

$$W(t) = \frac{1}{8} \cdot \underbrace{\int_{z=0}^{H} MOE(z) \cdot A(z) \cdot \varepsilon(z,t)^2 \cdot dz}_{\text{bending}}$$

$$+ \underbrace{\frac{1}{2} \cdot \int_{z=0}^{H} G(z) \cdot A_S(z) \cdot \gamma(z,t)^2 \cdot dz}_{\text{shearing}}, \quad (4)$$

where the bending and shear strains ε and γ are obtained from Eq. (2). In the plastic domain (Ib and Id), dW is independent of the ε- and γ-values. Therefore, the energy intensities per strain increment $dW/d\varepsilon$ for Ib and Id are equal to those for Ia and Ic at $\varepsilon = \varepsilon_1$ and $\gamma = \gamma_1$, respectively. The image series are again useful to verify that the stem section has not been broken off before the defined failure limits ($\varepsilon = 2.4\varepsilon_1$ or $\gamma = 1.4\gamma_1$) are exceeded. If necessary, the factors (2.4 and 1.4) are corrected to suit the failure mechanisms observed in the image series. No correction was required for the Norway spruce trees that we tested.

Energy is required to accelerate the stem because of its inertia (II, Table 3). For the x-ways deflection, this is described as:

$$dW = \frac{\pi}{4} \cdot \int_0^H D_1(z)^2 \cdot \rho_w(z) \cdot \frac{d^2x}{dt^2}(z) \cdot dx(z) \cdot dz. \quad (5)$$

Energy is absorbed and dissipated by the woody stem as the trolley front (simulated rock edge) penetrates it and crushes the wood fibers (III, Table 3):

$$dW = k_p \cdot x_p \cdot dx_p; \quad k_p = a_p \cdot D_1(z), \quad (6)$$

where k_p is penetration stiffness, $a_p = 10$ N mm^{-2} is a regression coefficient obtained experimentally (Step 7, Table 2) for 25 stems of Norway spruce from the test plot, x_p is penetration depth into the woody stem and $k_p \cdot x_p$ is penetration force. The value of k_p also includes the flattening of the stem caused by the high cross-sectional pressure in the impact direction. The sign of dW turns negative by the end of the trolley front–stem contact because of reflected elastic strain energy.

Energy, related to deformation, gravity and friction, is required to rotate the root–soil system (IV, Table 3):

$$dW = M^0(\phi) \cdot d\phi, \quad (7)$$

where $M^0(\phi)$ is the curve describing the resistive turning moment of the root–soil system as a function of the stem-base inclination ϕ, predicted with m_{tree}, DBH and H (Lundström et al. 2007b), and ϕ equals dx/dz ($z = 0$) (Eq. (1)). The beginning of the calculated $M^0(\phi)$-curve is compared with the curve measured for $0° < \phi < 2.5°$ in investigation no. 3 (Step 3, Table 2). If the difference is significant, the calculated $M^0(\phi)$ is rescaled in the M^0- or ϕ-direction, or both, to fit the measured $M^0(\phi)$. Rescaling was unnecessary for the Norway spruce trees that we tested.

Energy is required to accelerate the root–soil system in rotation because of its inertia (V, Table 3):

$$dW = J \cdot \frac{d^2\phi}{dt^2} \cdot d\phi;$$

$$J = \sum_{\substack{i=1 \\ V_{part}}}^{i=n} \left(J(z_i) + m_i \cdot z_i^2 \right), \quad (8)$$

where $d^2\phi/dt^2$ is the angular acceleration of the root–soil plate and J describes its mass moment of inertia, $J(z_i)$ is the J for the rotation around the axis $(x, z) = (0, z_i)$, of a horizontal, elliptical root–soil plate slice of thickness $z_{i+1} - z_i$, located at a distance z_i from $(x, y, z) = (0, 0, 0)$, with a mass m_i calculated from the bulk density ρ_s of the root–soil plate. The root–soil plate shape is modeled with an elliptical cross section and a depth-dependent taper. The part bent-off at the root–soil plate hinge is ignored (cf. the illustration in Lundström et al. 2007a). For all Norway spruce trees tested, ρ_s was estimated to be 1500 kg m^{-3} based on a soil density = 1900 kg m^{-3}, a root density = 700 kg m^{-3} and an assumed volume mix of soil (67%) and roots (33%) in the root–soil plate, similar to that for mature Norway spruce trees growing on mineral soils (Hakkila 1972). Because the root diameter decreases from the root–soil plate center outward, the root–soil plate stiffness decreases radially. Therefore, as estimated from series of digital images, only 70% of the entire volume of the root–soil plate V is considered to effectively contribute to its inertia during the impact. The 'participating' volume of the root–soil plate (V_{part}) is thus obtained by multiplying the height, width and depth of V by $0.7^{1/3}$.

The energy required to deform the root–soil system in translation (VI, Table 3) is:

$$dW = \frac{k_t}{\cos(\beta_s)} \cdot dx, \qquad (9)$$

where k_t represents the (unknown) translational deformation stiffness of the root–soil plate and β_s is the slope at the location of the tree. A hypothesis supported by tests is that k_t is independent of x and is equivalent to a force of shear-friction type (unit Newton). The magnitude of k_t is the difference between W_{app0} and W (I to VI + VIII) divided by the translational deformation of the root–soil plate at the end of T_{abs}.

Energy is required to accelerate the root–soil system in translation due to inertia (VII, Table 3):

$$dW = \frac{V_{part} \cdot \rho_s}{\cos^2(\beta_s)} \cdot \frac{d^2x}{dt^2} \cdot dx. \qquad (10)$$

Finally, the energy attributed to the group of energy absorption phenomena entitled 'Diverse losses' (VIII, Table 3) includes some minor energy quantities absorbed during T_{abs} through subsidiary phenomena not considered in the other groups. Principally, three observations from the test series help interpret this group: (1) The impact force involves a vertical component directed downward along the stem (Figure 3B) toward the root–soil system, to which the vertical structure of the stem base–root system reacts elastically and plastically. The x- and z-wise projections of Eq. (3) are used to analyze this feature, whose energy absorption is entirely attributed to the stem. (2) Because of the deflection at impact height, a downward displacement of the stem above impact height occurs. This displacement, which first accelerates and then decelerates, absorbs some energy due to inertia. (3) The simplified stress–strain relationships used for bending (cf. *Tree model and its mechanical properties*) will imply some fluctuations in time of the energy absorbed in Group VIII.

Energy absorption capacity of the tree

The energy absorption capacity, W_{cap}, of the tree is reached when the weakest component, i.e., either the stem or the root–soil system, in the transport of forces from the impact trolley to the ground fails (cf. Figure 3). To determine when and where during the impact this weak mechanical link occurs, observations were made on three levels (Table 4). From these, W_{cap} can be obtained, provided that the total kinetic energy of the trolley W_{app0} exceeds W_{cap}. If, however, W_{app0} falls below W_{cap}, the mechanical behavior of the tree that was tested needs to be extrapolated. Here, experimental experience has shown that the energy absorption related to phenomenon I (I, Table 3) is useful, because this energy in most cases dominates W_{cap} among the phenomena I–VIII, and the resistance related to phenomenon I governs the total possible energy uptake of the tree. Therefore, W_{app0} is multiplied by a factor equal to: the area under the defined $\sigma(\varepsilon)$-curve, between $\varepsilon = 0$ and $2.4\varepsilon_1$ divided by the area under the $\sigma(\varepsilon)$-curve between $\varepsilon = 0$ and the maximum measured ε. For example, with a stem deflection that yields (Eq. (2)) a maximum measured $\varepsilon = 2\varepsilon_1 = (1.4 + 0.6)\varepsilon_1$, the factor equals $(1.4/2 + 1.0)/$

Table 4. Observations relating to specific groups of energy involved in the trolley–tree interaction which help quantify the energy absorption capacity W_{cap} of the tree.

No.	Energy group: observation and interpretation
1	Energy intensity applied by the trolley in the x'-direction (Eq. (3)): an abrupt drop in this intensity to a value close to zero indicates a sudden low resistance offered by the tree to the impact loading, and the point of absorption capacity
2	Stem-bending (I): the measured maximum bending strain $\varepsilon(z, t)$ along the stem is compared to the stress–strain curves defined for bending (cf. *Tree model and its mechanical properties*). W_{cap} is reached at complete stem failure, i.e., when $\varepsilon(z, t) > 2.4\varepsilon_1(z, t)$. Stem failure is not caused by $\gamma(z, t) > 1.4\gamma_1(z, t)$ alone, but it sets off greater $\varepsilon(z, t)$
3	Root–soil rotation (IV): the measured stem-base rotation $\phi(t)$ is compared to the predicted $M^0(\phi)$ of the tree (Eq. (7)). The W_{cap} is reached when $\phi(t) > \phi(M^0_{max})$

(1.4/2 + 0.6) = 1.31. If, exceptionally, little stem curvature but large stem-base rotation occurs during the impact, the up-scaling factor is based on (3) in Table 4 in analogy with the $\sigma(\varepsilon)$-curve. Regardless of whether W_{app0} exceeds or falls below W_{cap}, the series of digital images are essential in assessing stem deflections and qualitatively surveying the interaction between the trolley front (simulated rock) and the heterogeneous tree structure.

Results

Tree reaction to the impact: general

The trolley hit the stems of the 15 test trees under somewhat different conditions (Table 5). The overall tree reactions during the impact, however, were similar in many ways. The trolley front crushed the wood fibers locally and pushed the stem down slope. This push bent the stem and also caused the root–soil system to rotate and translate. The trolley was rapidly stopped as a result of the absorption of its energy by the tree, but the tree reactions continued for a long time. The impact excited several different vibrational modes in the tree, causing transverse waves to propagate toward the tree top along the stem (Figure 4A). Above a certain tree height (about 12 m; Figure 4A), the energy contained in such a wave increased deflection of the stem, because stem diameter decreases with height, and thus stem rigidity and mass also decrease. Consequently, the strains and stresses associated with stem-bending increased. Close to the tree top, these strains and stresses exceeded the wood-failure limits, resulting in one or several stem failures. About 0.2 s after the predominant transverse wave had snapped the stem, the first natural

swaying frequency of the tree dominated its motion. Then one of the following scenarios occurred: (1) the swaying was gradually damped out and the tree remained standing; (2) the stem broke off at impact location and the tree part above this height fell; or (3) the root–soil system failed (in rotation and translation) and the entire tree fell, including the root–soil plate. Scenarios 2 and 3 occurred a few seconds after the first contact between the trolley and the tree stem. The types of tree failure observed are listed in Table 5.

The stem deflections during the trolley–stem interactions for all of the tested trees were accurately described by a ninth degree polynomial (Eq. (1)) or higher. The high polynomial degrees were required to describe the curvature of the lowermost and the uppermost stem, and thus the strains and stresses there. The highest strain rates for the stem and the root system occurred shortly after $t = 0$ ms. For the stem in shear, tension and compression, the strain rates never exceeded $1\ \mathrm{s^{-1}}$, and for the roots subjected to rotation and translation, they were even lower. Thus, the influence of strain rates on the stress–strain curve for the stem and on the turning moment for the root–soil system can be ignored.

Tree reaction and energy absorption: detail

Among the 15 trees tested, Tree A8 displayed typical reactions and energy absorptions. For this reason, and to demonstrate the method, the results for Tree A8 are presented in detail. On the basis of the stem deflections over time (Figure 4A and C), some significant tree reactions were identified: (1) the predicted shear failure of the stem ($\gamma = 1.4\gamma_1$) was reached at the stem base when (t, z, x) = (21 ms, 1.8 m, 120 mm); (2) the predicted bending failure of the stem ($\varepsilon = 2.4\varepsilon_1$) was reached at $z = 2.1$ m

Table 5. Data for the trolley and observations of tree failures resulting from the impact test. Abbreviations: m = mass; v = speed; z = height on the tree; β = angle to the horizontal; $_0$ refers to time zero, i.e., the first contact between the trolley front and the stem of the test tree; W_{app0} = kinetic energy of the trolley; x_{pr} = the remaining maximum depth of the local penetration of the trolley front into the woody tree stem; R = root–soil system; S = stem and R/S = predominantly R.

| Site and tree no.	Trolley						Tree	
	m (kg)	v_0 (m/s)	z_0 (m)	z_0/H (%)	β_0 (°)	W_{app0} (kJ)	x_{pr} (mm)	Failure type
A1	692	17.7	0.83	3.2	27	108	68	R
A2	692	18.4	1.10	3.3	27	118	60	S
A3	692	19.5	0.72	2.4	30	131	75	R
A4	792	20.0	0.95	2.8	26	158	56	R/S
A5	792	18.5	1.20	4.3	26	135	50	R
A6	492	5.7	1.20	5.8	26	8	20	S
A7	492	13.7	1.16	5.0	29	46	35	S
A8	592	13.3	1.36	5.3	28	52	44	S
A9	792	17.7	1.40	4.1	30	124	50	R/S
A10	792	20.7	1.48	4.6	27	170	70	S
B1	892	15.8	1.85	5.9	32	111	28	S
B2	892	17.5	0.70	2.1	33	136	75	R/S
B3	592	22.0	0.90	2.7	33	143	68	S
B4	492	21.5	1.80	5.6	33	113	35	S
B5	492	19.8	0.95	3.0	35	96	40	S
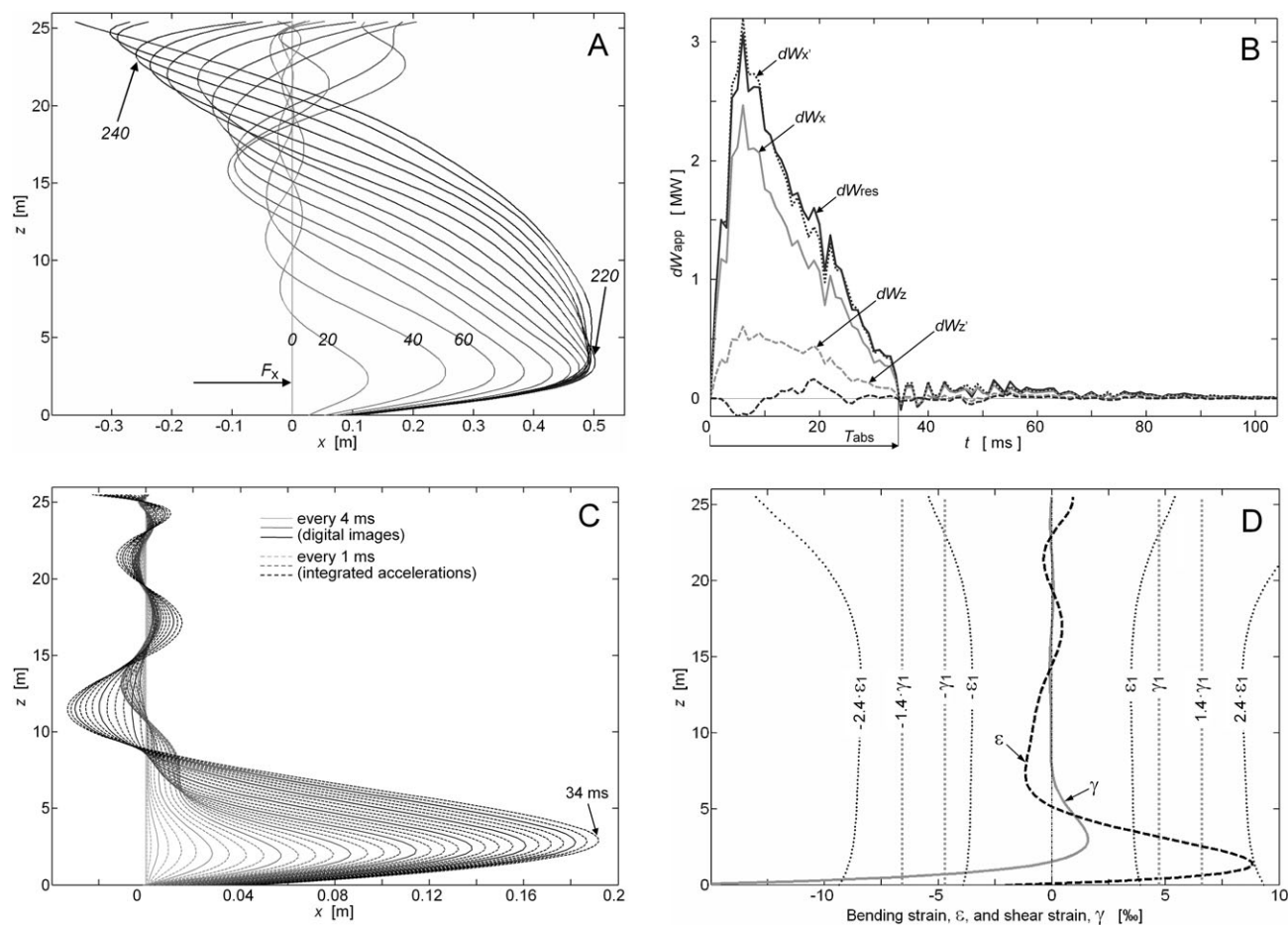
Figure 4. (A) Dependence of stem deflections x on height z and time $t = 0, 20, 40, \ldots, 300$ ms, where $t = 0$ is the time of the first contact between the force F applied by the trolley on the stem. Down slope is to the right. At $t = 220$ ms and maximum $x = 500$ mm, the trolley and the stem at impact height started to go backwards, in negative x'- and x-directions. (B) Energy intensity dW applied by the trolley to the tree. Abbreviations: dW_{res} is the vectorial sum of the intensities along and perpendicular to the trolley $dW_{x'}$ and $dW_{z'}$, respectively; and dW_x and dW_z are the resulting intensities across and along the stem (cf. Figure 3B). The period of energy absorption T_{abs} lasts from $t = 0$ to $t = 34$ ms as dW_{res} declines to a value close to zero. (C) Stem deflections during T_{abs} obtained from high-speed digital images (every 4 ms); completed with double integrated acceleration records (every 1 ms). (D) Stem strains at $t = 34$ ms, with the limits of plastification ($\pm\varepsilon_1$ and $\pm\gamma_1$) and of failure ($\pm 2.4\varepsilon_1$ and $\pm 1.4\gamma_1$). The stem had just reached the limit of bending failure at impact height, and shear failure was surpassed at the stem base. After $t = 34$ ms, ε and γ greatly increased along the upper part of the stem, and at $t = 160$ ms they both exhibited an hourglass shape similar to the $\pm 2.4\,\varepsilon_1$-curves. The width of this hourglass increased with time at the tree top and exceeded the $2.4\,\varepsilon_1$-limit at $(z, t) = (22.1$ m, 240 ms) (cf. A).

when $(t, z, x) = (34$ ms, 2.1 m, 190 mm) (cf. Figure 4D), which was at the same time as the rotation of the root–soil system was 5.4° and its translation was 45 mm; (3) the predicted $(M^0_{max}, \phi) = (69$ kNm, 6.3°) was reached when $(t, z, x) = (45$ ms, 2.2 m, 240 mm); (4) the maximum stem deflection was reached when $(t, z, x) = (220$ ms, 2.9 m, 500 mm), which was at the same time as the maximum rotation and translation of the root–soil system (9.0° and 85 mm) and (5) at $t = 240$ ms and $z = 22.1$ m (cf. Figure 4A), a transverse wave snapped the stem, because the bending strain was about 0.010.

Tree A8 fell on impact during the test, indicating that the kinetic energy applied by the trolley exceeded the energy absorption capacity of the tree. The latter could thus be determined from the energy intensity (dW_{res}) applied by the trolley to the tree and the development of the bending and shear stresses over time (nos. 1 and 2 in Table 4). At $t = 34$ ms, dW_{res} reached a value close to zero (Figure 4B, based on Eq. (3)). This was due to the low rate of deceleration of the trolley because the tree no longer offered much resistance to the moving trolley at $t = 34$ ms. The low resistance was caused by stem-bending failure at impact height and to stem shear failure at the stem base, resulting from the excessive bending and shear stresses, respectively (Figure 4D). The latter became evident when the stem was sawn into sections after the impact experiment and the wood fell apart longitudinally and cylindrically along the inner annual rings. By $t = 34$ ms, the trolley had trans-
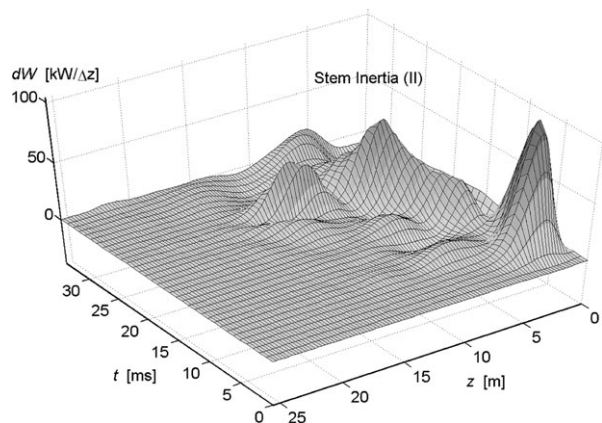
Figure 5. Energy absorption as a function of time and tree height $dW(t, z)$ for the stem and crown due to their x-wise acceleration (inertia). Abbreviations: $\Delta z = 25.5$ cm corresponds to 1% of the total tree height; negative dW-values indicate stem deceleration. For this tree (A8), the peak intensity of 110 kW/Δz occurred just below impact height, at stem height $z = 1.5$ m and time $t = 6$ ms. The energy absorption due to stem-bending (I) was distributed analogously.

mitted 96% (50 kJ) of its initial kinetic energy (52 kJ) to the tree. The absorption capacity W_{cap} of the tree was thus 50 kJ, which was exceeded by $52 - 50 = 2$ kJ or 4%. Until $t = 34$ ms, > 99.5% of the energy had been absorbed by the tree in the x–z-plane and < 0.5% in the y-direction.

How W_{cap} was assimilated by the tree becomes apparent when observing its energy absorption in different dimensions: (1) according to time and height, for individual phenomena (Figure 5); (2) according to time, for several phenomena (Figure 6); or (3) according to phenomenon, as relative parts of W_{cap} (Table 6). For Tree A8, W_{cap} was dominated by the stem's capacity to absorb energy (Figure 6). The energy absorption by the stem was principally a result of bending in the plastic domain, but the energy absorbed in shear deformation caused by bending cannot be ignored (Figure 6B). Energy absorption by the root–soil system was temporarily dominated by inertia energy, but energy absorption due to strain dominated toward the end of T_{abs} (Figure 6C). The energy absorbed through 'Diverse losses' (VIII, Figure 6D) equaled the energy 'Applied' minus 'Tree' (Figure 6A) minus 'VI' (Figure 6C), and was $50.0 - 46.3 - 2.5 = 1.2$ kJ at $t = 34$ ms. The bending of branches, caused by transverse waves along the upper stem, occurred mainly after T_{abs} and could therefore be neglected in the analysis of W_{cap}.

If the total aboveground energy absorption (I–IV) is analyzed according to height, < 5% of the absorption in Tree A8 occurred above $z = 9.0$ m (Figure 7), i.e., in the upper two-thirds of the tree. Thus, only the lower third of the stem contributed to the energy absorption capacity of the tree. Analyzed in time, the above- and the belowground energy absorption displayed a general and steady increase during
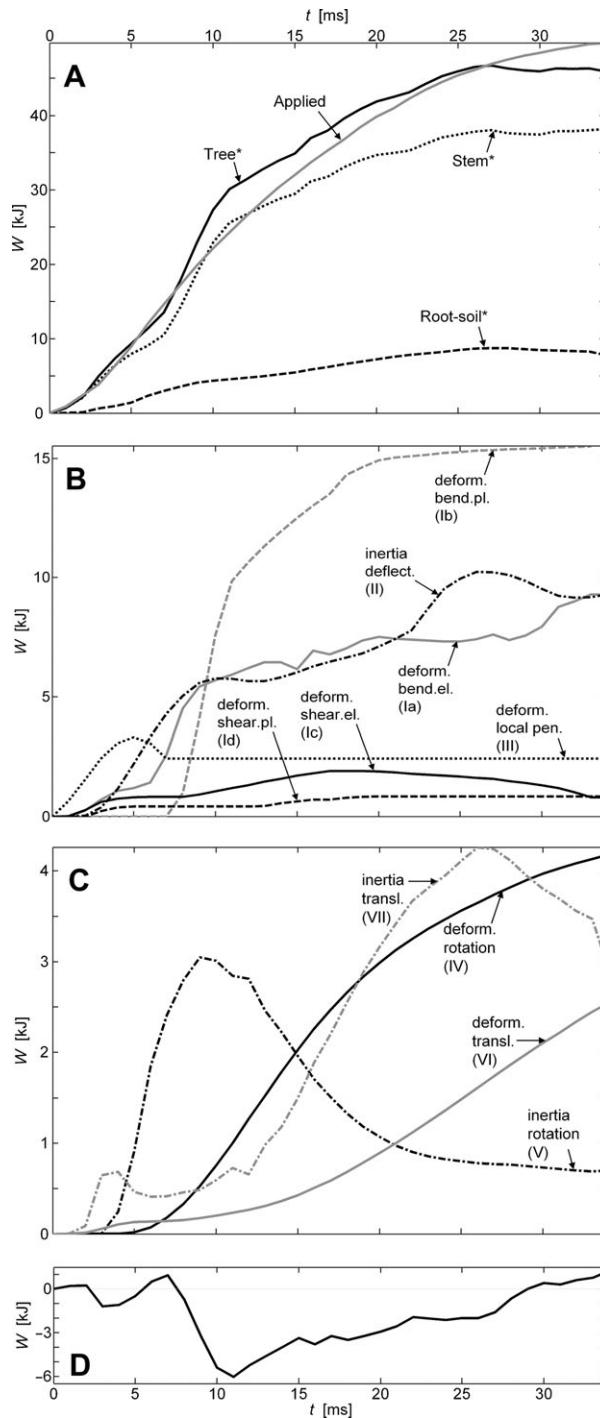

Figure 6. Energy intensities accumulated over time $W(t)$ in Tree A8. (A) The $W(t)$ applied by the trolley and $W(t)$ absorbed by the entire tree, the stem and the root–soil system without (*) considering the energy absorption phenomena VI and VIII. (B) The $W(t)$ for the stem in detail, where el. = elastic and pl. = plastic. (C) The $W(t)$ for the root–soil system in detail. (D) The $W(t)$ for 'Diverse losses' (VIII) (abbreviations are explained in Table 3).

the impact event (Figure 8), contributing 79% and 21%, respectively, of the energy capacity of the tree W_{cap} at $t = 34$ ms.

Table 6. Relative contributions of groups of energy absorption phenomena (I–VIII) to the energy absorption capacity W_{cap} of the tree, the relative contributions of the crown and stem (above ground) and the root–soil system (below ground), the absolute values of W_{cap}, and its ratio to the total energy applied by the impact trolley to the tree W_{app0}. The last row shows mean values for all trees.

Site and tree no.	Stem			Root–soil system				Tree	Total			
	Deform. bending I (%)	Inertia deflect. II (%)	Deform. local pen. III (%)	Deform. rotation IV (%)	Inertia rotation V (%)	Deform. transl. VI (%)	Inertia transl. VII (%)	Diverse losses VIII (%)	Above ground (%)	Below ground (%)	W_{cap} (kJ)	$\frac{W_{cap}}{W_{app0}}$ (–)
A1	49	8	6	12	4	10	9	3	65	35	90	1.2
A2	53	14	6	9	3	9	6	1	74	26	131	0.9
A3	43	10	11	11	3	10	8	4	67	33	169	0.78
A4	48	10	7	10	6	9	8	2	67	33	226	0.7
A5	56	16	3	9	4	4	5	3	77	23	129	1.05
A6	50	20	6	12	1	5	3	3	78	22	11	0.75
A7	55	13	5	11	3	7	6	2	74	26	54	0.85
A8	53	19	5	8	1	5	6	2	78	22	50	1.04
A9	59	14	4	8	2	5	5	3	79	21	137	0.9
A10	56	14	5	12	3	4	3	2	77	23	162	1.05
B1	60	22	1	13	1	0	0	3	84	16	96	1.15
B2	50	13	7	7	2	12	9	2	71	29	128	1.06
B3	53	12	7	13	3	6	5	2	73	27	159	0.9
B4	63	18	1	15	1	1	0	1	83	17	98	1.16
B5	51	16	4	13	3	5	4	3	73	27	139	0.69
All	53[1]	15	5	11	3	6	5	2	75	25	119	0.94

[1] On average, composed of 19% pure elastic bending (Ia), 31% plastic bending (Ib), 1.6% elastic shearing (Ic) and 1.7% plastic shearing (Id).

Energy absorption of the trees: summary

The energy absorption in time and space occurred generally in a similar way for all 15 trees. The vertical distribution of energy, however, was influenced by the relative impact height z_0/H. The magnitude of absorption for the different phenomena (I–VII) depended on z_0/H in a linear or logarithmic way. The correlations (R) between z_0/H and the relative energy absorption (Table 6) for the absorption groups were: aboveground, $R = 0.79$; I, $R = 0.66$; II, $R = 0.79$; III, $R = -0.71$; IV, $R = 0.32$; V, $R = -0.52$; VI, $R = -0.78$ and VII, $R = -0.75$. Clearly, the trees absorbed more energy above- than belowground if the impact occurred above a stem height of 0.70 m. Low relative impact height shifted the absorption from the stem (and crown) toward the root–soil system.
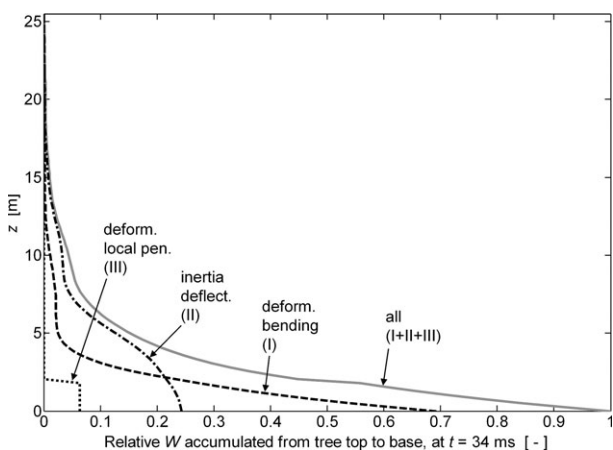

Figure 7. Height-wise (z) energy absorption by the stem of Tree A8 at the end of T_{abs}, i.e., at $t = 34$ ms, including local penetration of the trolley front into the woody stem (III), inertia due to x-wise acceleration of stem and branches (II) and stem-bending (I). The x-graduation is the energy accumulated z-wise, starting at the tree top and ending at the stem base, divided by the total energy (I + II + III) absorbed at $t = 34$ ms.
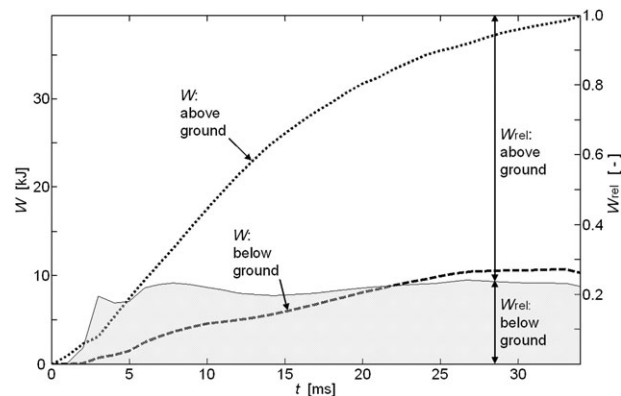

Figure 8. Development over time t of the tree's absolute energy absorption W above- and belowground for Tree A8, and the respective energy absorptions relative to the sum of the absolute values, W_{rel}.

system. The kinetic energy of the trolley exceeded W_{cap} for seven test trees and was below W_{cap} for the other eight trees (Table 6). For all trees, the translational stiffness of the root–soil system (cf. Eq. (9)) was best described by $k_t = 1.53 \times 10^6 DBH^3$ ($R^2 = 0.52$).

On the basis of the tree characteristics (Table 1) and W_{cap} (Table 6) of the tested tree, the predicted energy capacity of tree $W_{cap,p}$ could be well described with four models (Table 7). If the models of $W_{cap,p}$ described by DBH^α (nos. 2 and 4) were optimized for a low standard error $SE(Y_i - Y_{pi})$, instead of a high R^2, the exponent took the value $\alpha = 2.16$. Changing the exponent value in Model 1 did not improve its quality. For identical DBH and z_0/H, the W_{cap} of trees at Site A was on average 5% lower than the W_{cap} of trees at Site B (Figure 9), but the difference was statistically insignificant ($P = 0.37$). Tree A7, which had signs of rot in the center of the stem base, had a W_{cap} 30% lower than that predicted by Model 1.

Discussion

Our analysis of trees impacted by simulated rockfalls combines and makes use of: (1) information on the mechanical properties of tree components, such as the stem and the root–soil system subject to bending (Lundström et al. 2007b, 2008b); (2) a simplified tree model built from such components and (3) stem deflections in time assessed from digital images. The method provides results in sufficient detail to understand how a tree reacts and absorbs energy during a rock impact, which were the two main aims of the study. The third objective was to explore the energy absorption capacity W_{cap} of the tree. Here, the energy of the trolley W_{app0} should ideally exceed the energy absorption capacity W_{cap} of the tree by a few percent, to avoid extrapolation of the tree's mechanical behavior, where W_{cap} can be predicted statistically (e.g., Table 7) or mechanically (tree model). If only W_{cap} is required, W_{app0} should exceed W_{cap} with a larger margin, and attention should be paid to the additional inertia forces induced.

Tree mechanical properties contributed to uncertainty with respect to all three aims of our study. Minimizing this uncertainty requires detailed investigations of the tree before and after the impact experiment (cf. Table 2). Less information is known about how the root–soil system deforms in translation, even after this study. To improve the impact experiment, we suggest filming the trolley–tree interaction at a higher image frequency than that in our study with at least the same pixel resolution. Other full-scale experiments for exploring the tree–rockfall interaction have been used at a more coarse level of detail (Dorren and Berger 2006) or described rather briefly (Mizuyama and Narita 1988), making it difficult to compare methods.

Our observations confirm the complex behavior of a tree during a rock impact. Nevertheless, the mechanical behavior of the tree is logical and includes no strange or unex-

Table 7. Four regression models describing the energy absorption capacity W_{cap} of the tree. Abbreviations: Y = response variable (kJ); subscript p refers to predicted value; X = explanatory variable (basic unit is m); $\ln(b)$ = intercept, in the de-logarithmic model as $W_{cap} = b \cdot DBH^{a1}$; a = regression coefficient; $\boldsymbol{a}$ = standardized regression coefficient and $|\boldsymbol{a_1}/\boldsymbol{a_2}|$ = the impact of the first model variable X_1 on Y_i relative to the impact of the second variable X_2 on Y_i. Values of Y_i and X_j are listed top down according to their ranking (R^2) and contribution ($|\boldsymbol{a_j}|$) to the model, respectively. Significance: [*], $P < 0.05$; [**], $P < 0.01$ and [***], $P < 0.001$.

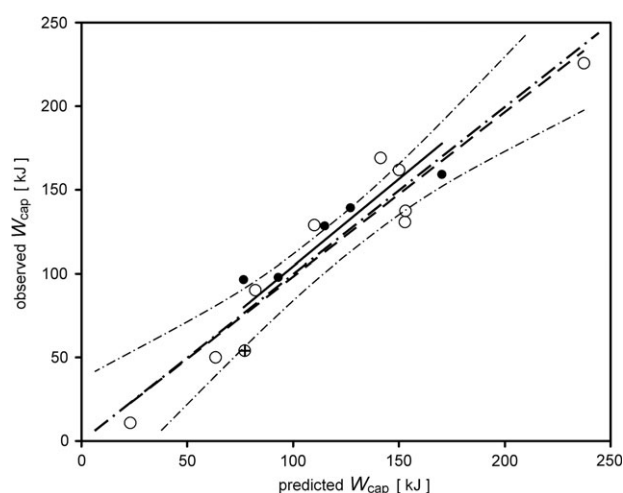| Model					Variables				
i	Y_i	$SE(Y_i)$	$SE(Y_i - Y_{pi})$	R^2	X_j	a_j	$\boldsymbol{a_j}$	$|\boldsymbol{a_1}/\boldsymbol{a_2}|$	$SE(X_j)$
1	W_{cap}	14.0	17.3	0.90	DBH^2	9.02E + 02[***]	4.53	3.15	0.070
					$DBH^2(z_0/H)$	−7.15E + 03[**]	−1.44	–	0.003
2	$\ln(W_{cap})$	0.191	0.269	0.88	$\ln(DBH)$	3.01E + 00[***]	3.63	–	0.229
					$\ln(b)$	7.25E + 00[***]	–	–	–
3	W_{cap}	14.0	20.6	0.87	DBH^2	7.72E + 02[***]	3.87	6.38	0.070
					z_0	−2.39E + 01[*]	−0.61	–	0.355
4	W_{cap}	14.0	23.5	0.81	DBH^2	6.40E + 02[***]	3.21	–	0.070

Figure 9. Observed energy absorption capacity W_{cap} plotted against the predicted W_{cap} for the ten Norway spruce trees at Site A (unfilled dots) and the five trees at Site B (filled dots) with linear regressions (continuous and dash lines, respectively). The dash-dot lines show the linear regression (heavy) and the bounds for a 95% confidence interval (fine) for all 15 trees. The tree with rot in the center of the stem base (A7) is indicated with a '+' in the circle.

pected phenomena. Because our impact experiment was labor-intensive, it would be worthwhile attempting to simulate rock–tree interactions with computer models, provided that the mechanical properties of the tree components involved in the major energy absorption phenomena (I–VII) are sufficiently well known. For this purpose, a suitable method to assess the translational deformation properties of the tree anchorage would be of great value. Additional full-scale tests are needed to calibrate phenomena that are not investigated in this work, such as other impact speeds and different impact shapes. A combination of in situ and computer experiments with tree–rock interactions should help increase the precision of estimates of how much protection forests can provide against rockfall and thus improve management strategies.

A tree's energy absorption capacity W_{cap} is effectively a combination of several phenomena. For all the Norway spruce trees tested, W_{cap} was largely dominated by the energy absorption in the stem (Table 6) and in general was restricted by bending stresses at the impact location (Figure 4D). When a tree is subject to typical impact heights under natural conditions (above 1.0 m in our study, Perret et al. 2004), the stem is decisive because it mobilizes much of the energy absorbed and it provides the weakest link in the transport of the impact force to the ground. Stem diameter has the greatest impact on W_{cap}, whereas the bending strengths and density of the stem are less relevant. The root–soil anchorage seems to provide the weakest link only if the tree is impacted at a low stem height and if it grows in a shallow soil (Table 5). The trees that are more firmly anchored than the trees that we tested would mobilize more energy absorption in the root–soil system when impacted at a low stem height. As a consequence of the stiffer stem base, more energy would also be absorbed through the local stem penetration of the rock front. It is, however, improbable that this penetration would be a limiting factor for the tree's capacity to absorb energy, similar to stem-bending (cf. Figure 4D and Table 5), unless the impacting rock edge is sharp enough to crosscut the stem.

We defined the energy absorption capacity W_{cap} of a tree as the maximum kinetic energy a tree can withstand without falling over. Provided that the tree recovers from the impact after a while, it can still continue to fulfil its protection function. If the tree falls, the energy absorption capacity is higher, because more of the energy related to the strain and inertia of the stem and of the root–soil system can be mobilized. The energy dissipation for *Abies alba* (Mill.) with a DBH = 0.40 m when completely destroyed by a rock was estimated (Dorren and Berger 2006) to be about 160 kJ. The corresponding W_{cap} of the *P. abies* in our study was about 100 kJ. It is likely that this 60 kJ difference is partly because the *A. alba* tree was better anchored than the *P. abies* tree that we tested. The difference in energy absorption for the root–soil system subject to rotation was about 50% (Stokes et al. 2005, Lundström et al. 2007*b*).

When selecting a prediction model for the energy absorption capacity of a tree, one should consider not only the statistical behavior of the linear regression model, but also the expected mechanical behavior of the tree–rock interaction. The strain and inertia energies absorbed in the stem are proportional to the woody stem diameter to the second and the third power, respectively, and the energy absorbed in the root–soil system subject to rotation is proportional to the DBH to the third power. How these energies are mobilized will depend on the height, speed and angle of the rock impact. This was taken into account for the models in Table 7, as far as the available data allowed. Whether the four models are valid beyond the range for which they were tested ($0.2 <$ DBH < 0.6 m and $z_0/H < 0.1$) is uncertain. What is striking is that the models including z_0 yield negative W_{cap} values for high impacts. This is understandable because the relationship between W_{cap} and z_0/H is logarithmic (Jonsson 2007) and not linear. It will be difficult to find a general allometric model that can precisely predict the energy absorption along the whole stem. However, trees clearly have a significant braking effect on falling rocks, and this study has contributed to our understanding of this effect. The findings should contribute to more precise rock–forest interaction models, thus improving the basis for managing protection forests.

Acknowledgments

References

Azzoni, A. and M.H. Defreitas. 1995. Experimentally gained parameters, decisive for rock fall analysis. Rock Mech. Rock Eng. 28:111–124.

Bragov, A. and A.K. Lomunov. 1997. Dynamic properties of some wood species. J. Phys. IV 7:487–492.

Brüchert, F., G. Becker and T. Speck. 2000. The mechanics of Norway spruce [*Picea abies* (L.) Karst]: mechanical properties of standing trees from different thinning regimes. For. Ecol. Manag. 135:45–62.

Chau, K.T., R.H.C. Wong and J.J. Wu. 2002. Coefficient of restitution and rotational motions of rockfall impacts. Intl. J. Rock Mech. Min. Sci. 39:69–77.

Chopra, A.K. 1995. Dynamics of structures: theory and applications to earthquake engineering. Prentice Hall, Englewood, NJ, 729 p.

Clough, R.W. and J. Penzien. 1993. Dynamics of structures. 2nd Edn. McGraw-Hill, New York, 738 p.

Cook, R.D., D.S. Malkus and M.E. Plesha. 2002. Concepts and applications of finite element analysis. 4th Edn. Wiley, New York, 719 p.

Dinwoodie, J.M. 2000. Timber: its nature and behaviour. 2nd Edn. E&FN SPON, London, 257 p.

Dorren, L.K.A. and F. Berger. 2006. Stem breakage of trees and energy dissipation during rockfall impacts. Tree Physiol. 26:63–71.

Dorren, L.K.A. and A.C. Seijmonsbergen. 2003. Comparison of three GIS-based models for predicting rockfall runout zones at a regional scale. Geomorphology 56:49–64.

FAO. 1998. Soil map of the world. Revised legend. *In* World Soil Resources Report, Vol. 60. FAO-UNESCO, Food and Agriculture Organisation, United Nations, Rome, 119 p.

Hakkila, P. 1972. Mechanized harvesting of stumps and roots. Commun. Inst. For. Fenn., Helsinki, 71 p.

Heidenreich, B. and V. Labiouse. 2004. Small-scale experimental study of rockfall impacts on granular slopes. Riv. Ital. Geotecnica 38:80–91.

Jonsson, M.J. 2007. Energy absorption of trees in a rockfall protection forest. Monogr. Swiss Federal Institute of Technology, Zürich, 209 p.

Jonsson, M.J., A. Foetzki, M. Kalberer, T. Lundström, W. Ammann and V. Stöckli. 2006. Root–soil rotation stiffness of Norway spruce (*Picea abies* L. Karst) growing on subalpine forested slopes. Plant Soil 285:267–277.

Jonsson, M.J., A. Foetzki, M. Kalberer, T. Lundström, W. Ammann and V. Stöckli. 2007. Natural frequencies and damping ratios of Norway spruce (*Picea abies* (L.) Karst) growing on subalpine forested slopes. Trees 21:541–548.

Kollmann, F.F.P. 1968. Principles of wood science and technology. *In* Solid Wood, Vol. 1. Springer-Verlag, Berlin, 592 p.

Krummenacher, B. and H.-R. Keusen. 1997. Steinschlag-Stutzbahnen – Modell und Realität. Proc. Société Suisse de Mécanique des sols et des roches, réunion d'automne, Montreux, pp 17–23.

Lundström, T., T. Jonas, V. Stöckli and W. Ammann. 2007*a*. Anchorage of mature conifers: resistive turning moment, root–soil plate geometry, and orientation of root growth. Tree Physiol. 27:1217–1227.

Lundström, T., M.J. Jonsson and M. Kalberer. 2007*b*. The root–soil system of Norway spruce subjected to turning moment: resistance as a function of rotation. Plant Soil 300:35–49.

Lundström, T., T. Jonas and A. Volkwein. 2008*a*. Analysing the mechanical performance and growth adaptation of Norway spruce using a nonlinear finite-element model and experimental data. J. Exp. Bot. 59:2513–2528.

Lundström, T., M. Stoffel and V. Stöckli. 2008*b*. Fresh-stem bending of silver fir and Norway spruce. Tree Physiol. 28:355–366.

Mizuyama, T. and H. Narita. 1988. Debris flow control by woods and their impact energy absorptivity. Proc. Interpraevent, Graz, pp 173–181.

Murray, Y.D. 2003. Development of a wood material model for roadside safety applications. Aptek Inc., Colorado Springs, pp 1–10.

Perret, S., M. Baumgartner and H. Kienholz. 2004. Rockfall injuries in mountain forests – a method for data collection and analysis. Proc. Interpraevent, Riva/Trient, V, pp 87–98.

Polomski, J. and N. Kuhn. 2001. Wurzelhabitus und Standfestigkeit der Waldbäume. Fortswiss. Centralbl. 120:303–317.

Stoffel, M., A. Wehrli, R. Kuhne, L.K.A. Dorren, S. Perret and H. Kienholz. 2006. Assessing the protective effect of mountain forests against rockfall using a 3D simulation model. For. Ecol. Manage. 225:113.

Stokes, A., F. Salin, A.D. Kokutse, S. Berthier, H. Jeannin, S. Mochan, L. Dorren, N. Kokutse, M. Abd Ghani and T. Fourcaud. 2005. Mechanical resistance of different tree species to rockfall in the French Alps. Plant Soil 278:107–117.

Sundström, B. 1998. Handbok och formelsamling i Hållfasthetslära, Vol. 1. Department of Solid Mechanics, Royal Institute of Technology, Stockholm, Department of Solid Mechanics, Royal Institute of Technology, 398 p.

Wessolly, L. and M. Erb. 1998. Handbuch der Baumstatik und Baumkontrolle. Patzer, Berlin, 270 p.

Zinggeler, A., B. Krummenacher and H. Kienholz. 1991. Steinschlagsimulation in Gebirgswäldern 3, Berichte und Forschungen, Geographisches Institut, Univ. Freiburg, pp 61–70.

Appendix

Table A1. List of the symbols and notations used in the study and their definitions and units.

Notation	Description	Unit
A, A_s	Cross-sectional area of the woody stem and its effective shear area	m^2
B	Double bark thickness	m, mm
β_s; β_0	Slope of the soil; angle to the horizontal of the impact direction on the tree	°
D_1, D	Stem diameter over and under bark	m, mm
DBH	Stem diameter over bark at breast height ($z = 1.3$ m)	m, cm
dW	Energy intensity	$J\ s^{-1}$, W, kW
ε; ε_1	Stem-bending strain (without the contribution from shear deformation); value at which the behavior changes from ideal-elastic to ideal-plastic	–
ϕ	Rotation of the root–soil system around the y-axis	rad, °
G	Modulus of shearing elasticity along the stem	MPa
γ; γ_1	Shear strain along the stem; value at which the behavior changes from ideal-elastic to ideal-plastic	–
H	Tree height	m
I	Cross-sectional moment of inertia of the woody stem	m^4
k_p	Penetration stiffness for the trolley front into the woody stem	$N\ mm^{-1}$
k_t	Translational stiffness of the root–soil system pushed along the slope (cf. Eq. (9))	N
M^0; M^0_{max}	Resistive turning moment around the y-axis of the root–soil system; maximum M^0	MPa
MOE	Modulus of bending elasticity of the stem cross section	MPa, GPa
m_{tree}	Total aboveground tree mass	kg
ρ_w	Bulk density of the fresh stem on bark	$kg\ m^{-3}$
RW; $_{i,o}$	Width of annual rings; reference to the mean of the inner 75% radial part of the stem cross section and to the mean of the remaining outer part	mm
σ, σ_{max}	Bending stress and strength of the stem cross section	MPa
t	Time after the first contact between the trolley and the tree	s, ms
T_{abs}	Period from $t = 0$ until the intensity of the tree's energy absorption reaches a value close to zero	s, ms
τ, τ_{max}	Shear stress and strength of the stem section in the direction along the stem	MPa
V; V_{part}	Volume of the root–soil plate; the V that effectively contributes to inertia during the impact	m^3
W	Energy	J, kJ
W_{cap}; $W_{cap,p}$	Energy absorption capacity of the tree, being the maximum W_{app0} a tree can withstand without falling over; the predicted W_{cap}	J, kJ
W_{app}; W_{app0}	Kinetic energy applied be the impact trolley on the tree; W_{app} at time zero	J, kJ
x, y, z	Tree coordinates: origin at stem base; $x =$ horizontal stem deflection; $z =$ height above origin (cf. Figure 3A)	m
x', y', z'	Local coordinates of the impact trolley: origin at its center of gravity; $x' =$ impact direction; $z' =$ upward (cf. Figure 3B)	m
I, II, ..., VIII	Denominations for groups of energy absorption phenomena (cf. Table 3)	